

# Kinetic Modeling and Process Analysis for Photo-Production of $\beta$ -Carotene in *Dunaliella Salina*

Yimei Xi

Dalian University of Technology

Jiali Zhang

Dalian University of Technology

Fantao Kong (✉ [kongfantao@dlut.edu.cn](mailto:kongfantao@dlut.edu.cn))

Dalian University of Technology <https://orcid.org/0000-0003-2847-2838>

Jian Che

Dalian University of Technology

Zhanyou Chi

Dalian University of Technology

---

## Research

**Keywords:** *Dunaliella salina*, Dynamic kinetic modelling, Cultivation optimization, Environmental factors,  $\beta$ -carotene production

**Posted Date:** November 3rd, 2021

**DOI:** <https://doi.org/10.21203/rs.3.rs-1017195/v1>

**License:**  This work is licensed under a Creative Commons Attribution 4.0 International License.

[Read Full License](#)

---

**Version of Record:** A version of this preprint was published at Bioresources and Bioprocessing on January 17th, 2022. See the published version at <https://doi.org/10.1186/s40643-022-00495-6>.

1                   **Kinetic Modeling and Process Analysis for Photo-Production of**  
2    **$\beta$ -Carotene in *Dunaliella salina***

3  
4 Yimei Xi<sup>a,c</sup>, Jiali Zhang<sup>b</sup>, Fantao Kong<sup>c\*</sup>, Jian Che<sup>c,d\*</sup>, Zhanyou Chi<sup>c</sup>

5  
6 <sup>a</sup> Key Laboratory of Industrial Ecology and Environmental Engineering (Ministry of  
7 Education, China), School of Environmental Science and Technology, Dalian  
8 University of Technology, Dalian 116024, China

9 <sup>b</sup> School of Mathematical Sciences, Dalian University of Technology, Dalian 116024,  
10 China

11 <sup>c</sup> School of Bioengineering, Dalian University of Technology, Dalian 116024, China

12 <sup>d</sup> Dalian Xinyulong Marine Biological Seed Technology Co. Ltd., Dalian 116200,  
13 China

14  
15 \*Corresponding authors:

16 Fantao Kong

17 Tel: +86-15642336188

18 E-mail: [kongfantao@dlut.edu.cn](mailto:kongfantao@dlut.edu.cn)

19  
20 Jian Che

21 Tel: +86-18604261385

22 E-mail: [jianche82@dlut.edu.cn](mailto:jianche82@dlut.edu.cn)

23  
24

25 **Abstract:**

26 *Dunaliella salina* is a green alga with the great potential to generate natural  
27  $\beta$ -carotene. However, the corresponding mathematical models to guide optimized  
28 production of  $\beta$ -carotene in *Dunaliella salina* is not yet available. In this study,  
29 dynamic models were proposed to simulate effects of environmental factors on cell  
30 growth and  $\beta$ -carotene production in *D. salina* using online monitoring system.  
31 Moreover, the identification model of the parameter variables was established, and an  
32 adaptive particle swarm optimization algorithm based on parameter sensitivity  
33 analysis was constructed to solve the premature problem of particle swarm algorithm.  
34 The proposed kinetic model is characterized by high accuracy and predictability  
35 through experimental verification, which indicates its competence for future process  
36 design, control and optimization. Based on the model established in this study, the  
37 optimal environment factors for both  $\beta$ -carotene production and microalgae growth  
38 were identified. The approaches created are potentially useful for microalgae  
39 cultivation and high-value compounds production.

40

41 **Key words:** *Dunaliella salina*, Dynamic kinetic modelling, Cultivation optimization,  
42 Environmental factors,  $\beta$ -carotene production

43

44

45

46

47 **Introduction:**

48 In the last decades, massive investments were done on microalgae industry, mainly  
49 due to their capacity to synthesize lipids for biofuel production or synthesize the  
50 carotenoid for high-value products production (Chew, 2017; Kong et al., 2018;  
51 Salome & Merchant, 2019).  $\beta$ -Carotene is a high-valued carotenoid pigment with  
52 wide applications in the cosmetic, pharmaceutical and food industries (Coppens et al.,  
53 2016; Gateau et al., 2017; Paillie-Jimenez et al., 2020). The supply of natural  
54  $\beta$ -carotene still falls short of demand at present, since  $\beta$ -carotene has high antioxidant  
55 activity and significant impact on animal pigmentation (Henriquez et al., 2016). To fill  
56 this gap, green alga *Dunaliella salina* has been chosen as one of the best candidates  
57 for  $\beta$ -carotene production due to its high  $\beta$ -carotene content (up to 10%) (Benamotz et  
58 al., 1982; Xi et al., 2020a).

59 Microalgae require macronutrients and micronutrients for photosynthesis, which are  
60 important for growth and product accumulation. The optimal temperature and light  
61 are also critical for rapid metabolism and biomass productivity in microalgae  
62 (Alexandre Viruela, 2021; del Rio-Chanona et al., 2017). During the past years, many  
63 studies have been carried out to evaluate the optimal operating conditions for  
64  $\beta$ -carotene production in microalgae. For example, high irradiance, high temperature,  
65 oxidative stress and nitrogen-deprivation have been found to significantly stimulate  
66 the accumulation of  $\beta$ -carotene in microalgae (Fachet et al., 2016; Wu et al., 2016;

67 Kim et al., 2013). Although there are extensive indoor measurements for the  
68 microalgae system (Zhu et al., 2021; Zhu et al., 2018b), much less effort has been  
69 focused on the modelling of these stages and determine the optimal operating  
70 conditions. To optimize reactor design and predict its performance, understanding of  
71 simultaneous effects of different environmental and operational variables on  
72 microalgae culture is necessary. Mathematical models can be used to study the effects  
73 of the environmental and operational variables, which are related to the output  
74 variables (e.g., biomass productivity and bio-product production), allowing the effect  
75 of changing the input variables to be studied without the need for individual  
76 experimental tests (Alexandre Viruela, 2021; del Rio-Chanona et al., 2018). In order  
77 to successfully conduct process control and make optimization, it is essential to  
78 construct a highly accurate kinetic model, which can be capable of well predicting the  
79 dynamic behavior of the underlying biosystem. Meanwhile, model-based process  
80 design is also considered to be one of the most effective tools to accomplish the  
81 transfer of bioprocess from laboratory short-term scale to industrial long-term scale  
82 (Alexandre Viruela, 2021; del Rio-Chanona et al., 2017). Despite its importance,  
83 model-based process design for  $\beta$ -carotene production still remains to be elucidated.

84 Previous modeling studies have taken on the specific challenge of modeling growth in  
85 algae systems. Although some dynamic models have been constructed to simulate this  
86 process. However, most of the environmental parameters have not been considered in  
87 biokinetics in those models, which limited their application. For example, a  
88 photobioreactor model that deals only with both light and nitrogen limitation has been

89 proposed through Beer-Lamberts Law and the Droop Equation, respectively (Bernard,  
90 2009). Microalgae growth is reported to be related to light intensity and the  
91 intracellular nitrogen concentration or quota, but the effect of other relevant  
92 parameters such as temperature or inorganic carbon concentration which restrict the  
93 applicability of Microalgae have not been included. Mathematical model have been  
94 used to predict and optimize the microalgae biomass and astaxanthin production, and  
95 specific variables including light intensity, temperature, retention time and nutrients  
96 concentration have been used to monitor the process performance and construct  
97 models (Zhang et al., 2015; Zhang et al., 2016). However, due to the specificity  
98 between microalgae species and the induction stage of carotenoid, where cells stop  
99 growing and carotenoid commences to accumulate is very difficult to model.

100 Droop, Monod and Andrew models have been extensively applied to predict biomass  
101 growth rate under a single substrate or nutrient condition, such as phosphorus (del  
102 Rio-Chanona et al., 2017), nitrogen (del Rio-Chanona et al., 2017; Liu et al., 2018),  
103 carbon(Straka & Rittmann, 2019) and light (Holdmann et al., 2018; Zhang et al.,  
104 2015). Previous models are able to accurately estimate biomass productivity when the  
105 temperature is within a range of values enabling microalgae growth (Zhang et al.,  
106 2016). Integrated experimental-computational frameworks that have the ability to  
107 predict biomass growth and product accumulation under different growing conditions,  
108 which will help to optimize the process performance, operating conditions and  
109 scale-up of cultivation systems for commercialization and industrial applicability  
110 (Zerriouh et al., 2017).

111 Nevertheless, kinetic modelling of simultaneous co-limitation of growth media  
112 elements (e.g, nitrogen and carbon) and environmental factors (e.g, light and  
113 temperature) has not been reported yet. Additionally, while carotenoid accumulation  
114 has been considered to be proportional to biomass growth, the effects of abiotic stress  
115 towards enhancement of carotenoid productivity have been recently shown through a  
116 new kinetic model considering biomass growth and carotenoid accumulation as two  
117 different dynamic variables (Zhang et al., 2016). Dynamic simulation is an effective  
118 tool to determine the optimal operating conditions for both laboratory scale and  
119 industrial scale carotenoid production processes. However, the previous models are  
120 only able to accurately estimate biomass productivity when the temperature is within  
121 a range of values enabling microalgae growth (Jiang et al., 2015). Moreover, the  
122 previous models can only predict biomass and bio-compounds production when the  
123 incident light intensity is within a range of constant, but the average light intensity  
124 received by the cells in the PBRs is underestimated (Lamers et al., 2010).

125 To accurately simulate the dynamic process of the  $\beta$ -carotene induction stage, the  
126 current study aims to construct rigorous models including the effects of temperature,  
127 average light intensity, carbon and nitrogen source on algal growth and  $\beta$ -carotene  
128 accumulation, which to the best of our knowledge has not been reported at present.  
129 Furthermore, a sensitivity analysis was conducted to simulate various parameters on  
130 microalgae production process. The relationship between  $\beta$ -carotene accumulation  
131 and algal growth has also been comprehensively studied in this study, which are  
132 potentially useful for microalgae cultivation and high-value compounds production.

## 133 **Material and Modeling Methodology**

### 134 **Microalgal strain and its preculture conditions**

135 The microalgae *D. salina* CCAP 19/18 was purchased from Culture Collection of  
136 Algae and Protozoa (Windermere, United Kingdom). The strain was maintained in the  
137 medium of optimized Artificial Sea Water (ASW), composing of 1.5 M NaCl, 5 mM  
138 KNO<sub>3</sub>, 0.45 mM MgCl<sub>2</sub>·6H<sub>2</sub>O, 0.05 mM MgSO<sub>4</sub>·7H<sub>2</sub>O, 0.3 mM CaCl<sub>2</sub>·2H<sub>2</sub>O, 0.13  
139 mM K<sub>2</sub>HPO<sub>4</sub>, 0.02 mM FeCl<sub>3</sub>, 0.02 mM EDTA, 1 mL of trace elements stock per liter  
140 with 50 mM H<sub>3</sub>BO<sub>3</sub>, 10 mM MnCl<sub>2</sub>·4H<sub>2</sub>O, 0.8 mM ZnSO<sub>4</sub>·7H<sub>2</sub>O, 0.8 mM  
141 CuSO<sub>4</sub>·5H<sub>2</sub>O, 2 mM NaMoO<sub>4</sub>·2H<sub>2</sub>O, 1.5 mM NaVO<sub>3</sub>, 0.2 mM CoCl<sub>2</sub>·6H<sub>2</sub>O and the  
142 pH was adjusted to 7.5 by addition of Tris-buffer (40 mM). *D. salina* was precultured  
143 in 500 mL conical flasks at 50 μmol·m<sup>-2</sup>·s<sup>-1</sup> light intensity.

### 144 **Operation of photobioreactor**

145 The microalgal cells at logarithmic phase were inoculated into a  
146 multi-device-equipped flat plate photobioreactor (also known as Algal Station), which  
147 can guarantee accurate and stable light condition control as we previously described  
148 (Cao et al., 2019). In the platform of Algal Station, the cultivation temperature was  
149 automatically controlled at 25°C, the pH was maintained at 7.5 by  
150 computer-controlled micro-addition of CO<sub>2</sub> in the bubbling air, and the cultures were  
151 agitated at 400 mL·min<sup>-1</sup> with filtered air (0.2 μm porosity membrane). The culturing  
152 broth was sampled daily for analysis of dry weight and β-carotene content. The  
153 incident photon flux density and transmitted photon flux were recorded online at 20  
154 min intervals. Each treatment was independently repeated three times.

155 **Analytical Methods**

156 **Growth analyses**

157 Cell density was determined spectrophotometrically using a UV/VIS  
158 spectrophotometer (Jasco V-530, Japan) at 680 nm. The microalgal dry weight (DW)  
159 was determined according to the method we previously described (Cao et al., 2019).  
160 Briefly, with pre-weighed Whatman GF/C filters, 10 mL culture broth was filtered and  
161 washed three times with 2 mL of 0.5 M ammonium bicarbonate, and then dried below  
162 60°C for over 16 h until the weight was constant. The DW of the microalgae cells was  
163 calculated, according to the difference between final and initial filter weights and  
164 volume of the filtered sample.

165 The microalgal growth rate ( $\mu_i$ , h<sup>-1</sup>) was calculated by Equation (1)

166 
$$\mu_i = \frac{\ln DW_i - \ln DW_{i-1}}{t_i - t_{i-1}} \quad (1)$$

167 where  $DW_i$  and  $DW_{i-1}$  (g·L<sup>-1</sup>) are the biomass concentration measured at time  $t_i$  and  
168  $t_{i-1}$ , respectively.  $t_i$  and  $t_{i-1}$  are hour  $i$  and  $i-1$  when the culture broth was sampled.

169  **$\beta$ -carotene content analysis**

170 The  $\beta$ -carotene content was determined by modified spectrophotometric method as  
171 we previously reported (Xi et al., 2020b; Zhu et al., 2018a). Briefly, one milliliter of  
172 cell suspension was centrifuged at 10,000 rpm for 2 min. After centrifugation, the  
173 supernatant was discarded, and 3 mL dodecane was added. The sample was shaken  
174 vigorously to re-suspend the algae pellets. Then, 9 mL of methanol was added to  
175 completely break up the cells and the tube was shaken vigorously again, then  
176 centrifuged for 2 min at 10,000 rpm. The dodecane-containing lipophilic carotenoids

177 (upper layer) were measured with a spectrophotometer (Jasco V-530, Japan) at 453  
 178 nm and 665 nm with dodecane as reference.  $\beta$ -carotene concentration was calculated  
 179 using Eq. (2):

$$180 \quad C_{\beta\text{-car}} (\text{mg}\cdot\text{L}^{-1}) = (A_{453} - A_{665}/3.91) \times 3.657 \times 3 \times X \quad (2)$$

181 where:  $(A_{453} - A_{665}/3.91)$  is the absorbance of  $\beta$ -carotene corrected for chlorophyll  
 182 contamination, 3.657 is the calibration factor derived from HPLC analysis of  
 183  $\beta$ -carotene concentration, 3 is the number of milliliters of dodecane added for  
 184 extraction, and X is the dilution factor to measure absorbance on spectrophotometer.

185 The content of  $\beta$ -carotene in the algae biomass was calculated according to Eq. (3).

$$186 \quad \beta\text{-carotene } (\%) = \frac{C_{\beta\text{-car}} \times 10}{DW} \quad (3)$$

187 where:  $C_{\beta\text{-car}}$  is  $\beta$ -carotene concentration ( $\text{mg}\cdot\text{L}^{-1}$ ),  $\beta$ -carotene (%) is  $\beta$ -carotene  
 188 content, and DW is cell dry weight ( $\text{mg}\cdot\text{L}^{-1}$ ).

### 189 **Model construction methodology**

190 Currently, the types of kinetic models, namely the Monod model and the Droop  
 191 model (Zhang et al., 2015), are widely used for bioprocess simulation. Due to its high  
 192 accuracy and flexibility, the Monod model is selected and modified to simulate the  
 193 correlation between biomass growth and consumption of nitrate and carbon.

$$194 \quad \frac{dX}{dt} = \mu_0 * X - \mu_d * X^2 \quad (4)$$

$$195 \quad \mu_0 = \mu_{\max} (T, I, N, C) f(T) \left( \frac{I_{av}}{I_{av} + k_s + \frac{I_{av}^2}{k_i}} \right) \left( \frac{C}{K_C + C} \right) \left( \frac{N}{K_N + N} \right) \quad (5)$$

$$196 \quad f(T) = A * e^{-\frac{E_a}{R*T}} - B * e^{-\frac{E_b}{R*T}} \quad (6)$$

197 Where  $X$  is biomass concentration ( $\text{g} \cdot \text{L}^{-1}$ ),  $\mu_0$  is cell specific growth rate ( $\text{h}^{-1}$ ),  $\mu_{max}$  is  
 198 maximum cell specific growth rate ( $\text{h}^{-1}$ ),  $I_{av}$  is average light intensity,  $\mu_d$  is cell decay  
 199 rate ( $\text{h}^{-1}$ ),  $K_s$  is light saturation value produced by cell growth,  $K_i$  is photoinhibition  
 200 value of cell growth,  $A$  and  $B$  are the coefficients before the index,  $E_a$  is the activation  
 201 energy for cell growth,  $E_b$  is inactivation energy of cell growth,  $K_N$  is the nitrate  
 202 half-velocity constant, and  $K_C$  is carbon half-velocity constant.

203 Equation 4 simulates the biomass growth rate. Its first term on the right-hand side  
 204 represents biomass growth, and the second term represents cell respiration and decay.  
 205 In terms of  $\beta$ -carotene production, it was reported that the uptake of culture nitrate is  
 206 essential for cells to synthesize  $\beta$ -carotene (Lamers et al., 2012). Meanwhile, as  
 207  $\beta$ -carotene is a primary carotenoid, it can be consumed by cells for their growth and  
 208 converted to other metabolites when necessary. Therefore, Equation 7 is constructed  
 209 to simulate  $\beta$ -carotene production. In this equation, the first term on the right  
 210 represents  $\beta$ -carotene synthesis rate and is originated from the Monod model, while  
 211 the second term represents  $\beta$ -carotene consumption rate. So far there are no reports  
 212 about investigating the detailed metabolic mechanisms of  $\beta$ -carotene consumption.

213

$$214 \quad \frac{dw}{dt} = \left[ b + \left( 1 - \frac{K_{NW}}{N} \right) \right] * \frac{K_{NW}}{N} * \left( 1 - \frac{K_{CW}}{C} \right) * \frac{K_{CW}}{C} * \left( 1 - \frac{W}{W_{max}} \right) * \frac{I_{av}}{I_{av} + K_{sw} + \frac{I_{av}^2}{k_{iw}}} * \left[ A_w * e^{-\frac{E_{aw}}{R \cdot T}} - B_w * e^{-\frac{E_{bw}}{R \cdot T}} \right] \quad (7)$$

215 where  $W$  is  $\beta$ -carotene content,  $b$  is no correlation coefficient for the growth of  
 216  $\beta$ -carotene production,  $K_{sw}$  is the light saturation value of  $\beta$ -carotene accumulation,  
 217  $E_{aw}$  is activation energy of  $\beta$ -carotene accumulation;  $w_{max}$  is the maximum  $\beta$ -carotene  
 218 content,  $K_{NW}$  is nitrate half velocity constant for  $\beta$ -carotene synthesis,  $I_{av}$  is average

219 light intensity ( $\mu\text{mol}\cdot\text{m}^{-2}\cdot\text{s}^{-1}$ ),  $K_{iw}$  is  $\beta$ -carotene accumulation photoinhibition value,  
220  $K_{CW}$  is carbon content half velocity constant for  $\beta$ -carotene synthesis, and  $E_{bw}$  is  
221 inactivation energy for  $\beta$ -carotene synthesis.

## 222 **Parameter estimation methodology**

223 In order to obtain the best parameters of dynamic model that can fit the experimental  
224 data, it was take the average relative error between the experimental data and the  
225 system output as the objective function, and the range of biomass and  $\beta$ -carotene  
226 concentration as the state constraints, and then establish a nonlinear programming  
227 problem (NLP) for the parameter variables. Considering that the particle swarm  
228 optimization (PSO) is easy to be premature, this study used an adaptive PSO based on  
229 sensitivity analysis to solve the problem. This algorithm can ensure that the required  
230 parameters can reach the approximate global optimum, and has a certain degree of  
231 robustness. The implementation in this work is programmed in the MATLAB  
232 (R2021a) optimization environment.

233

234

## 235 **Results and Discussion**

### 236 **Effects of environmental factors on cell growth**

237 To examine the effect of temperature, light intensity, carbon and nitrate concentration  
238 on the growth kinetics of *D. salina*, different specific sets of experiments were carried  
239 out by cultivating the cells in PBRs under different temperature, average light  
240 intensity, initial concentrations of dissolved nitrates and carbons. The experiment was  
241 setup and then monitored daily up to a total cultivation time of 96 h, when the  
242 occurrence of exponential growth was observed.

243 It is found that temperature remarkably influence the rate of cell growth, cell decay  
244 and bioproduct accumulation. The optimal temperature can facilitate microbial  
245 biomass growth and bioproducts synthesis (del Rio-Chanona et al., 2017; Fachet et al.,  
246 2014; Guiheneuf & Stengel, 2017). The effect of temperature on the growth rate in *D.*  
247 *salina* is mainly reflected in the efficiency of photosynthesis and respiration (Fachet et  
248 al., 2014). The growth rate at different temperatures was shown in Figure 1A. At the  
249 range of 10-30°C, the growth rate was positively correlated with temperature, and  
250 when the temperature rises to 30°C, the growth rate begins to decrease. In the range of  
251 30-40°C, the growth rate has a negative correlation with temperature. The logarithmic  
252 growth phase of *D. salina* has the largest growth rate ( $0.164 \text{ h}^{-1}$ ) at the temperature of  
253 28 °C. The Arrhenius equation has been widely used to describe the effects of  
254 temperature on both biomass growth (Zhang et al., 2016). The parameters of the  
255 Arrhenius model can be obtained by model fitting under different range of  
256 temperatures.

257 Light intensity significantly affects biomass growth rates (Bonnefond et al., 2016). In  
258 general, the effect of light intensity on cell growth can be reflected by the Aiba model  
259 (del Rio-Chanona et al., 2017). In our experiments, the Aiba model was used to  
260 replace local light intensities by an average light intensity which was calculated by Eq.  
261 5 in a suspended reactor. The model parameters  $\mu_{max}$  and  $K_s$  were fitted as shown in  
262 Figure 1B, within a certain range of light intensity, the relationship between the  
263 average light intensity and the growth rate of *D. salina* conforms to the Aiba equation.  
264 The growth rate tends to increase with the increase of light intensity stable value when  
265 the light intensity exceeds  $379.6 \mu\text{mol}\cdot\text{m}^{-2}\cdot\text{s}^{-1}$ . According to the curve, the  
266 half-saturation constant of light ( $K_i$ ) is  $1705 \mu\text{mol}\cdot\text{m}^{-2}\cdot\text{s}^{-1}$ . It is indicated that in most  
267 of the cases, a higher average light intensity (up to  $600 \mu\text{mol}\cdot\text{m}^{-2}\cdot\text{s}^{-1}$ ) can result in a  
268 higher biomass growth rate, which is consistent with the observations published in  
269 previous studies (Bonnefond et al., 2016; Fachet et al., 2016).

270 When nitrogen concentration is the limiting factor, the relationship between the  
271 growth rate and the nitrogen concentration was shown in Figure 1C. The relationship  
272 between the nitrogen concentration and the growth rate of *D. salina* conforms to the  
273 Monod equation. The values of the model parameters  $\mu_{max}$  and  $K_N$  after fitting show  
274 that within a certain range of nitrogen concentration, the growth rate  $\mu$  of algal cells  
275 increased with the increase of the nitrogen concentration. The  $\mu$  tends to a stable value  
276 when the nitrogen concentration exceeds  $330 \text{mg}\cdot\text{L}^{-1}$ . In terms of the influence of  
277 nitrate concentration on biomass growth rate, in both sets of experiments nitrate  
278 concentration in the culture keeps increasing after the addition of dense nitrate

279 influent, which means that the consumption rate of nitrate due to biomass uptake was  
280 slower than its refreshment rate. By comparing biomass concentrations at the different  
281 sets of experiments, it seems that biomass growth rate was always higher in a denser  
282 nitrate concentration culture.

283 This tendency was also observed in the carbon experiments when the carbon content  
284 changes from 0 to 500 mM. Under the carbon limiting condition, the relationship  
285 between specific growth rate and carbon content was shown in Figure 1D. The  
286 relationship between the carbon concentration and the growth rate conformed to the  
287 Monod equation within a certain range of carbon content in *D. salina*. The growth rate  
288 (referred as  $\mu$ ) of the algae was improved as the increase of the carbon content when  
289 the carbon concentration was in a lower range. The  $\mu$  tended to a stable value with the  
290 increase of the carbon concentration when the carbon concentration exceeds 50 mM,  
291 above which a stable of final biomass concentration was obtained, and indicated a  
292 stable biomass growth rate. Therefore, the results was suggested that the high biomass  
293 growth rate obtained with nitrate concentration 500 mg·L<sup>-1</sup>, carbon concentration 50  
294 mM at 28°C and the average light intensity 600  $\mu\text{mol}\cdot\text{m}^{-2}\cdot\text{s}^{-1}$  (Figure 1).

### 295 **Effects of environmental factors on $\beta$ -carotene synthesis**

296 The  $\beta$ -carotene accumulation rate at different temperatures was shown in Figure 2A.  
297 We found that the  $\beta$ -carotene accumulation rate was negatively correlated with  
298 temperature at the range of 10-35°C, and when the temperature rises to 30°C, the  
299  $\beta$ -carotene accumulation begins to increase. In the range of 30-40°C, the  $\beta$ -carotene

300 accumulation rate has a positive correlation with temperature. The *D. salina* has the  
301 largest  $\beta$ -carotene accumulation rate at 10 °C, which was 0.095 h<sup>-1</sup>. The Arrhenius  
302 equation has been widely used to describe the effects of temperature on both  
303 bioproduct accumulation. The parameters of the Arrhenius model can be obtained by  
304 model fitting under different range of temperatures.

305 We found that in the different light intensity experiments,  $\beta$ -carotene content  
306 continuously increases with the raising average light intensity from 150 to 600  
307  $\mu\text{mol}\cdot\text{m}^{-2}\cdot\text{s}^{-1}$ , while its maximum value falls within the range of 300 to 480  
308  $\mu\text{mol}\cdot\text{m}^{-2}\cdot\text{s}^{-1}$  (Figure 2B). However, neither of the current observations were in  
309 agreement with the previous studies where  $\beta$ -carotene content was found to decrease  
310 with the increasing light intensity from 150 to 750  $\mu\text{mol}\cdot\text{m}^{-2}\cdot\text{s}^{-1}$  (Fachet et al., 2014).  
311 As a result, the distinct discrepancy between current observations and previous  
312 conclusions suggests the complex metabolic mechanisms of  $\beta$ -carotene synthesis. It  
313 also indicated that other factors apart from light intensity can significantly affect  
314 intracellular  $\beta$ -carotene content. In terms of the effect of nitrate concentration on  
315  $\beta$ -carotene synthesis, it was known that nitrate is essential for  $\beta$ -carotene synthesis,  
316 and  $\beta$ -carotene was a primary carotenoid which can be accumulated under  
317 nitrogen-sufficient conditions. The results showed that under the same light intensity,  
318  $\beta$ -carotene content in the experiments with lower nitrate concentration was higher  
319 than that in the experiments with higher culture nitrate concentration (Figure 2B).  
320 This phenomenon was also reported in a recent study where a similar photosynthetic  
321 pigment lutein was synthesized by *Desmodesmus sp.* under a nitrogen-sufficient

322 condition (del Rio-Chanona et al., 2017).

323 Therefore, the current observation indicated that  $\beta$ -carotene content was higher in a  
324 lower nitrate concentration condition could also be explained as what has been  
325 demonstrated for  $\beta$ -carotene. Under the carbon deprivation condition, the relationship  
326 between  $\beta$ -carotene accumulation and carbon concentration was shown in Figure 2D,  
327 within a certain range of carbon concentration, the relationship between the carbon  
328 concentration and the specific accumulation rate conformed to the Monod equation in  
329 *D. salina*. The  $\beta$ -carotene accumulation rate of the algae increased with the higher  
330 concentration of the carbon. The  $\mu$  tends to a stable value with the increase of the  
331 carbon concentration when the carbon concentration exceeds 200 mM.

332 For  $\beta$ -carotene production, it was found that a higher light intensity and a denser  
333 culture nitrate concentration can always lead to a higher  $\beta$ -carotene production as long  
334 as nitrate inhibition does not happen, as shown in Figure 2B. Such conflicting  
335 conclusion compared to that of  $\beta$ -carotene synthesis was reasonable, because  
336  $\beta$ -carotene production is the product of both biomass concentration and  $\beta$ -carotene  
337 intracellular content. Although a high nitrate concentration may limit  $\beta$ -carotene  
338 accumulation, it can significantly facilitate green algae biomass growth. Consequently,  
339 total  $\beta$ -carotene production can still be increased through this condition. Nonetheless,  
340 it should be noted that low  $\beta$ -carotene content can remarkably elevate the bioprocess  
341 downstream separation cost, which may seriously reduce the process profitability.  
342 Hence, it was essential to guarantee an adequate  $\beta$ -carotene content when aiming to  
343 maximize total  $\beta$ -carotene production.

## 344 **Results of dynamic model construction**

345 In order to construct a highly accurate dynamic model which is capable of simulating  
346 the performance of green algal  $\beta$ -carotene production, and accomplish further  
347 process optimization, it is vital to understand the biochemical kinetics of the  
348 investigated system. Especially for the current process, the temperature, light intensity,  
349 carbon content and culture nitrate concentration are included in the model since  
350 previous studies have declared that they are the main factors affecting  $\beta$ -carotene  
351 synthesis (Bonnetfond et al., 2016; Lamers et al., 2012). From the section 3.1 and 3.2,  
352 parameters in the kinetic model were calculated through single factor experiments as  
353 shown in Table 1. We found that the specific biomass decay rate not equal 0, which  
354 suggested that they have not negligible effects on the system. This can be attributed to  
355 the fact that in all the conducted experiments, biomass concentration kept steady until  
356 the end of the study, the effect of cell decay should not disguise. The parameters were  
357 used as the initial value of the parameter for further parameter identification.  
358 Considering that a single perturbation method may affect the accuracy of the results,  
359 in order to reduce the sensitivity of the parameters from the perturbation method, we  
360 randomly perturbs each parameter  $Q$  times, and draws a box plot of the objective  
361 function with respect to the perturbation percentage.

362 In the process of parameter simulation, the disturbances time  $Q = 100$ , disturbance  
363 range  $\zeta = 5\%$ , and the optimal parameters value of the system were obtained with the  
364 aid of the PSO algorithm. The optimized parameters resulted in a box plot of the  
365 objective function change under a certain perturbation percentage, as shown in the

366 Table 2, Figure 3 and Figure 4:  $E_b$ ,  $A_w$  and  $b$  obtains the minimum value of the  
367 objective function within the perturbation range of the corresponding parameter  $\pm 5\%$ ,  
368 and  $E_a$  decreases monotonically within the perturbation range of the parameter.  
369 However, within this range, the maximum difference of the objective function value is  
370  $0.016 \times 10^{-3}$ . It was suggested the system is not sensitive to changing the parameters,  
371 and the system reaches the approximate global optimal solution of the objective  
372 function at 0 perturbation of the parameters. The results show that the parameters  
373 obtained by the above algorithm can fit the experimental data well, and the parameters  
374 created in this study were an approximate global optimal solution of the nonlinear  
375 dynamic system and have certain robustness.

### 376 **Validation of dynamic model predictability**

377 To estimate the optimal operating conditions for long-term bioprocess optimization,  
378 besides accurately representing a known experiment, the model should possess great  
379 predictive capability when simulating unknown processes. For this reason, the  
380 predictive capability of the constructed model was investigated through two scenarios.  
381 In the first scenario, the model was used to predict the dynamic performance of a  
382 continuous illumination batch experiment lasting for 6 days indoors. In the second  
383 scenario, the model was applied to predict a light/dark cycle batch experiment lasting  
384 for 6 days under outdoor condition. Noticeably, due to the frequent change of light  
385 intensity, the second system becomes more complex and has a higher uncertainty  
386 compared to the first scenario. Both light intensity and initial nitrate concentration in  
387 these two experiments are different from those used for model construction. The

388 detailed operating conditions of these experiments are listed in Table 3.

389 To identify the predictability of current models for different *D. salina* strains  
390  $\beta$ -carotene production process, four additional experiments were carried out. The  
391 experiments have the initial biomass concentration of  $0.10 \text{ g}\cdot\text{L}^{-1}$ , with incident light  
392 intensity of 200, 600, 800 and  $1000 \mu\text{mol}\cdot\text{m}^{-2}\cdot\text{s}^{-1}$  and temperature of 20 and 25 °C.  
393 The model was validated by Algal station system with 1.0 L PBR, steady temperature  
394 and light intensity within the reactor operating conditions. Despite the added  
395 variability, the model was able to accurately reproduce the process performance with  
396 the same calibrated values for all the model parameters. The comparison between the  
397 current model simulation results and experimental data was examined. It was shown  
398 that the current models can accurately predict the dynamic performance of green algal  
399  $\beta$ -carotene production process with different operating conditions (Figure 5 and 6).  
400 Because the current dynamic model was constructed with the aim to predict the  
401 optimal operating conditions in future process design and control, it has to be  
402 characterized by not only high accuracy but also good predictability. Therefore, this  
403 model is used to simulate the dynamic performance of all the remaining four  
404 experiments conducted in this study. We found that the current model shows great  
405 predictability within a wide range of operating conditions throughout the entire  
406 experimental time course. Among the all experimental data points, the majority of  
407 deviation between model prediction and real experiment was far below 10%, with  
408 only four exceptions shown in Figure 5A (11.4%) and Figure 6C (13.8%). Therefore,  
409 it was strongly indicated the current model showed high predictability and accuracy of

410 the current model, as well as its great competence for further process design and  
411 optimal control.

412 Our model was fitted with experimental data that accounted for the most significant  
413 parameters that affect microalgae metabolism. Moreover, this model was intended to  
414 promote and assist the development of evaluation applications of microalgae at  
415 industrial level. Our model could also be used as a predictive tool to determine the  
416 combination of environmental and operational parameters that promote maximum  
417 biomass productivity in other microalgae.

## 418 **Conclusions**

419 In this study, a mathematical model was constructed to simulate the growth and  
420  $\beta$ -carotene production from *D. salina*. Sensitivity analysis showed that  $\beta$ -carotene  
421 synthesis is more sensitive to the operating parameters of the system than cell growth.  
422 Moreover, the accuracy and predictability of kinetic model were further verified.  
423 Based on the dynamic model, optimal light intensities for cell growth and  $\beta$ -carotene  
424 production were proposed. The established model has high accuracy and predictive  
425 capability, which is potentially useful for further application in process control and  
426 optimization during microalgae cultivation at industrial level.

## 427 **Authorship contribution statement**

428 YX, JC and ZC designed the research. YX and FK wrote the paper. FK, YX and JZ  
429 analyzed the data. YX and TL performed the research and provided technical support.  
430 All authors read and approved the final manuscript.

431 **Funding**

432 This work was supported by the National Natural Science Foundation of China  
433 (31900221), Natural Science Foundation of Liaoning Province of China  
434 (2020-MS-102), Fundamental Research Funds for the Central Universities  
435 (DUT21LK14), and Major and Special Program on Science and Technology Projects  
436 in Dalian City (2020ZD23SN009).

437 **Availability of data and materials**

438 Not applicable

439 **Declarations**

440 **Ethics approval and consent to participate**

441 Not applicable.

442 **Consent for publication**

443 Not applicable.

444 **Competing interests**

445 The authors declare that they have no competing interests.

446

447

448 **References**

- 449 Alexandre Viruela, S.A., Ángel Robles, Luis Borrás Falomir, Joaquín Serralta, Aurora Seco, José  
450 Ferrer. (2021) Kinetic modeling of autotrophic microalgae mainline processes for sewage  
451 treatment in phosphorus-replete and -deplete culture conditions. *Sci Total Environ* **797**,  
452 1-15.
- 453 Benamotz, A., Katz, A., Avron, M. (1982) Accumulation of beta-carotene in halotolerant algae -  
454 purification and characterization of beta-carotene-rich globules from *Dunaliella-bardawil*  
455 (chlorophyceae). *J Phycol* **18**, 529-537.
- 456 Bernard, O., Masci, P., Sciandra, A., . (2009) A photobioreactor model in nitrogen limited  
457 conditions. *MATHMOD 09 Vienna*, 1521–1530.
- 458 Bonnefond, H., Moelants, N., Talec, A., Bernard, O., Sciandra, A. (2016) Concomitant effects of  
459 light and temperature diel variations on the growth rate and lipid production of *Dunaliella*  
460 *salina*. *Algal Res* **14**, 72-78.
- 461 Cao, X.P., Xi, Y.M., Liu, J., Chu, Y.D., Wu, P.C., Yang, M., Chi, Z.Y., Xue, S. (2019) New insights  
462 into the CO<sub>2</sub>-steady and pH-steady cultivations of two microalgae based on continuous  
463 online parameter monitoring. *Algal Res* **38**,1-6.
- 464 Coppens, J., Grunert, O., Van den Hende, S., Vanhoutte, I., Boon, N., Haesaert, G., De Gelder, L.  
465 (2016) The use of microalgae as a high-value organic slow-release fertilizer results in  
466 tomatoes with increased carotenoid and sugar levels. *J Phycol* **28**, 2367-2377.
- 467 del Rio-Chanona, E.A., Ahmed, N.R., Zhang, D.D., Lu, Y.H., Jing, K.J. (2017) Kinetic modeling  
468 and process analysis for *Desmodesmus sp* lutein photo-production. *Aiche Journal* **63**,  
469 2546-2554.
- 470 del Rio-Chanona, E.A., Liu, J., Wagner, J.L., Zhang, D.D., Meng, Y.Y., Xue, S., Shah, N. (2018)  
471 Dynamic modeling of green algae cultivation in a photobioreactor for sustainable  
472 biodiesel production. *Biotechnol Bioeng* **115**, 359-370.
- 473 Fachet, M., Flassig, R.J., Rihko-Struckmann, L., Sundmacher, K. (2014) A dynamic growth model  
474 of *Dunaliella salina*: Parameter identification and profile likelihood analysis. *Bioresour*  
475 *Technol* **173**, 21-31.
- 476 Fachet, M., Hermsdorf, D., Rihko-Struckmann, L., Sundmacher, K. (2016) Flow cytometry  
477 enables dynamic tracking of algal stress response: A case study using carotenogenesis in

478 *Dunaliella salina*. Algal Res **13**, 227-234.

479 Gateau, H., Solymosi, K., Marchand, J., Schoefs, B. (2017) Carotenoids of Microalgae Used in  
480 Food Industry and Medicine. Mini-Reviews In Medicinal Chemistry**17**, 1140-1172.

481 Guiheneuf, F., Stengel, D.B. (2017) Interactive effects of light and temperature on pigments and  
482 n-3 LC-PUFA-enriched oil accumulation in batch-cultivated *Pavlova lutheri* using  
483 high-bicarbonate supply. Algal Res **23**, 113-125.

484 Henriquez, V., Escobar, C., Galarza, J., Gimpel, J. (2016) Carotenoids in Microalgae. Sub-cellular  
485 biochemistry **79**, 219-37.

486 Holdmann, C., Schmid-Staiger, U., Hornstein, H., Hirth, T. (2018) Keeping the light energy  
487 constant - Cultivation of *Chlorella sorokiniana* at different specific light availabilities and  
488 different photoperiods. Algal Res **29**, 61-70.

489 Jiang, H., Lin, X., Lei, M., Kong, X. (2015) Effects of Temperature on Growth, Astaxanthin  
490 Accumulation and Antioxidative Capacity in *Haematococcus pluvialis*. J Phycol **36**,  
491 63-68.

492 Kim, S.-H., Liu, K.-H., Lee, S.-Y., Hong, S.-J., Cho, B.-K., Lee, H., Lee, C.-G., Choi, H.-K. (2013)  
493 Effects of Light Intensity and Nitrogen Starvation on Glycerolipid, Glycerophospholipid,  
494 and Carotenoid Composition in *Dunaliella tertiolecta* Culture. Plos One **8**,1-10.

495 Kit Wayne Chew, J.Y.Y., Pau Loke Show, Ng Hui Suan, Joon Ching Juan, Tau Chuan Ling,  
496 Duu-Jong Lee, Jo-Shu Chang. (2017) Microalgae biorefinery: High value products  
497 perspectives. Bioresour Technol **229**, 53-62.

498 Kong, F., Romero, I.T., Warakanont, J., Li-Beisson, Y. (2018) Lipid catabolism in microalgae.  
499 New Phytologist **218**, 1340-1348.

500 Lamers, P.P., van de Laak, C.C.W., Kaasenbrood, P.S., Lorier, J., Janssen, M., De Vos, R.C.H.,  
501 Bino, R.J., Wijffels, R.H. (2010) Carotenoid and Fatty Acid Metabolism in Light-Stressed  
502 *Dunaliella salina*. Biotechnol Bioeng **106**, 638-648.

503 Lamers, P.P., Janssen, M., De Vos, R.C.H., Bino, R.J., Wijffels, R.H. (2012) Carotenoid and fatty  
504 acid metabolism in nitrogen-starved *Dunaliella salina*, a unicellular green microalga. J  
505 Phycol **162**, 21-27.

506 Liu, J., Yao, C.H., Meng, Y.Y., Cao, X.P., Wu, P.C., Xue, S. (2018) The Delta F/F-m '-guided  
507 supply of nitrogen in culture medium facilitates sustainable production of TAG in

508 *Nannochloropsis oceanica* IMET1. *Biotechnology for Biofuels* **11**,1-10.

509 Paillie-Jimenez, M.E., Stincone, P., Brandelli, A. (2020) *Front Sustain Food S* **4**,590-439.

510 Salome, P.A., Merchant, S.S. (2019) A Series of Fortunate Events: Introducing *Chlamydomonas* as  
511 a Reference Organism. *The Plant cell* **31**, 1682-1707.

512 Straka, L., Rittmann, B.E. (2019) Growth kinetics and mathematical modeling of *Synechocystis* sp.  
513 PCC 6803 under flashing light. *Biotechnol Bioeng* **116**, 469-474.

514 Wu, Z., Duangmanee, P., Zhao, P., Juntawong, N., Ma, C.H. (2016) The effects of light,  
515 temperature, and nutrition on growth and pigment accumulation of three *Dunaliella*  
516 *salina* strains isolated from saline soil. *Jundishapur Journal of Microbiology* **9**,1-6.

517 Xi, Y., Wang, J., Xue, S., Chi, Z. (2020a) beta-Carotene production from *Dunaliella salina*  
518 cultivated with bicarbonate as carbon source. *J Microbiol Biotechn* **30**, 868-877.

519 Zeriuoh, O., Reinoso-Moreno, J.V., Lopez-Rosales, L., Sierra-Martin, B., Ceron-Garcia, M.C.,  
520 Sanchez-Miron, A., Fernandez-Barbero, A., Garcia-Camachoa, F., Molina-Grima, E.  
521 (2017) A methodological study of adhesion dynamics in a batch culture of the marine  
522 microalga *Nannochloropsis gaditana*. *Algal Res* **23**, 240-254.

523 Zhang, D., Dechatiwongse, P., Hellgardt, K. (2015) Modelling light transmission, cyanobacterial  
524 growth kinetics and fluid dynamics in a laboratory scale multiphase photo-bioreactor for  
525 biological hydrogen production. *Algal Res* **8**, 99-107.

526 Zhang, D., Wan, M., del Rio-Chanona, E.A., Huang, J., Wang, W., Li, Y., Vassiliadis, V.S. (2016)  
527 Dynamic modelling of *Haematococcus pluvialis* photoinduction for astaxanthin  
528 production in both attached and suspended photobioreactors. *Algal Res* **13**, 69-78.

529 Zhu, C., Xi, Y., Zhai, X., Wang, J., Kong, F., Chi, Z. (2021) Pilot outdoor cultivation of an extreme  
530 alkalihalophilic Trebouxiophyte in a floating photobioreactor using bicarbonate as carbon  
531 source. *Journal of Cleaner Production* **283**,1-13.

532 Zhu, C., Zhu, H., Cheng, L., Chi, Z. (2018a) Bicarbonate-based carbon capture and algal  
533 production system on ocean with floating inflatable-membrane photobioreactor. *Journal*  
534 *of Applied Phycology* **30**, 875-885.

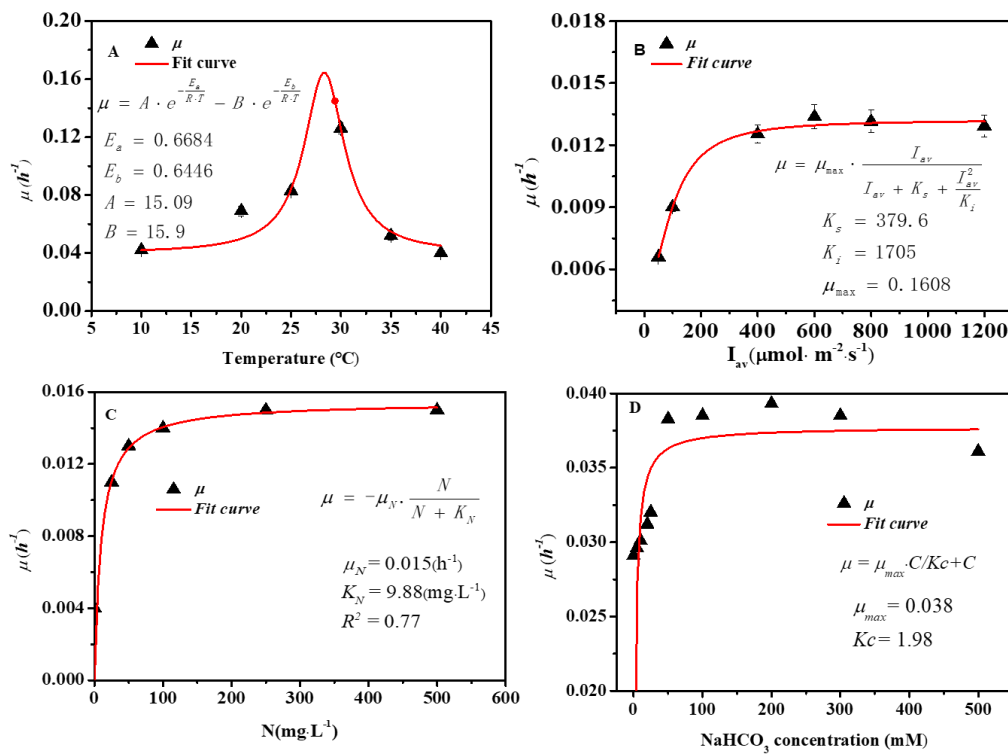
535 Zhu, C.B., Zhai, X.Q., Jia, J., Wang, J.H., Han, D.S., Li, Y.H., Tang, Y.J., Chi, Z.Y. (2018b)  
536 Seawater desalination concentrate for cultivation of *Dunaliella salina* with floating  
537 photobioreactor to produce beta-carotene. *Algal Res* **35**, 319-324.

538

539 **Figures**

540 **Figure 1.** Growth rate of *D. salina* under different culture conditions. (A) The  
541 relationship of temperature and cell specific growth rate (B) The relationship of light  
542 intensity and cell specific growth rate (C) The relationship of nitrogen concentration  
543 and cell specific growth rate (D) The relationship of carbon concentration and cell  
544 specific growth rate.

545



546

547

548

549

550

551

552

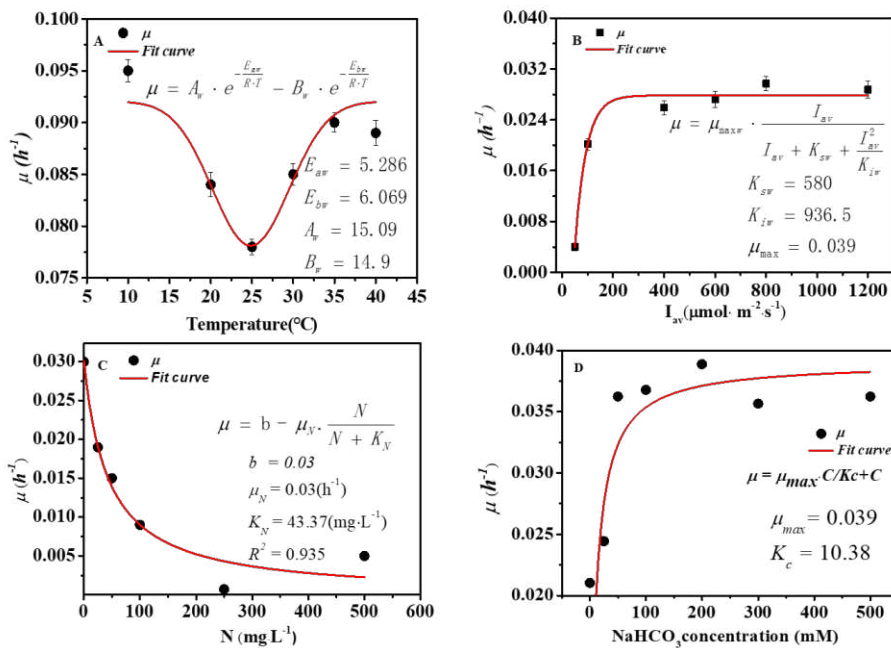
553

554

555

556

557 **Figure 2.**  $\beta$ -carotene accumulation rate of *D. salina* under different culture  
558 conditions. (A) The relationship of temperature and  $\beta$ -carotene accumulation rate (B)  
559 The relationship of light intensity and  $\beta$ -carotene accumulation rate (C) The  
560 relationship of nitrogen concentration and  $\beta$ -carotene accumulation rate (D) The  
561 relationship of carbon concentration and  $\beta$ -carotene accumulation rate.  
562



563

564

565

566

567

568

569

570

571

572

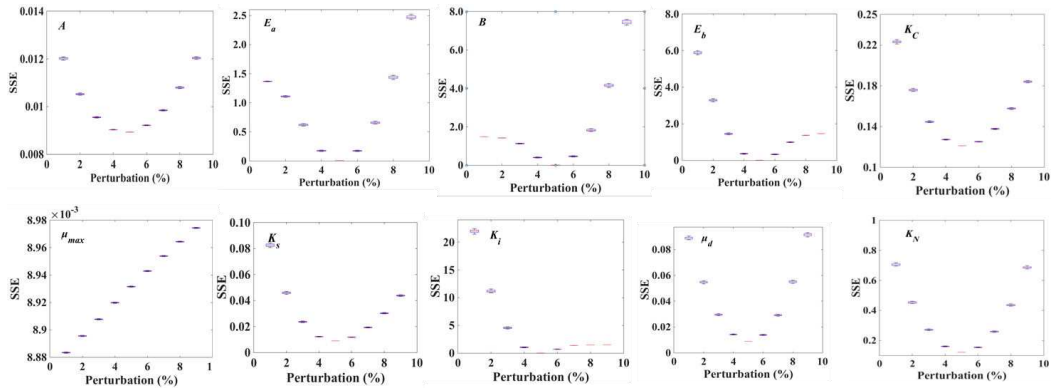
573

574

575

576 **Figure 3.** Optimization of model parameters for cell growth in *D. salina* (optimized  
577 by MATLAB). SSE: system squared error.

578



579

580

581

582

583

584

585

586

587

588

589

590

591

592

593

594

595

596

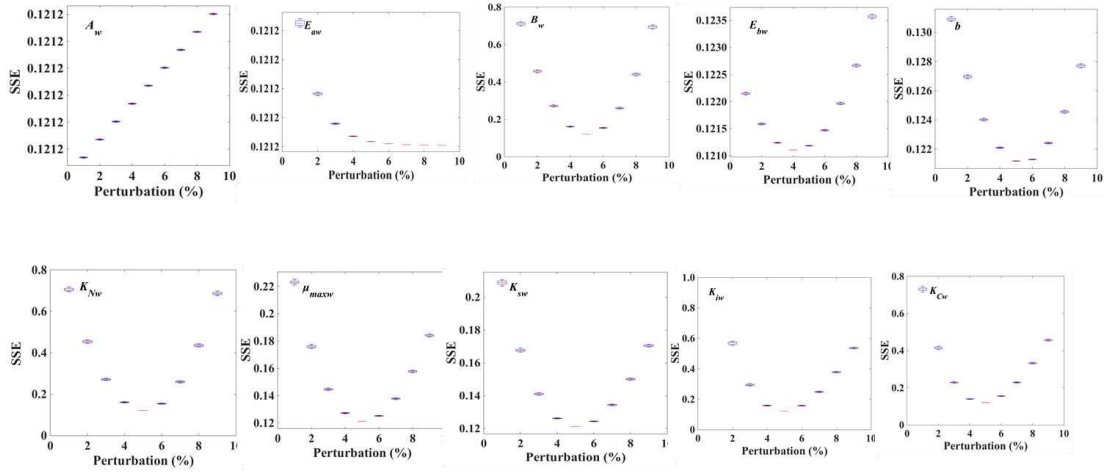
597

598

599

600 **Figure 4.** Optimization of model parameters for  $\beta$ -carotene accumulation in *D. salina*  
601 (optimized by MATLAB). SSE: system squared error.

602



603

604

605

606

607

608

609

610

611

612

613

614

615

616

617

618

619

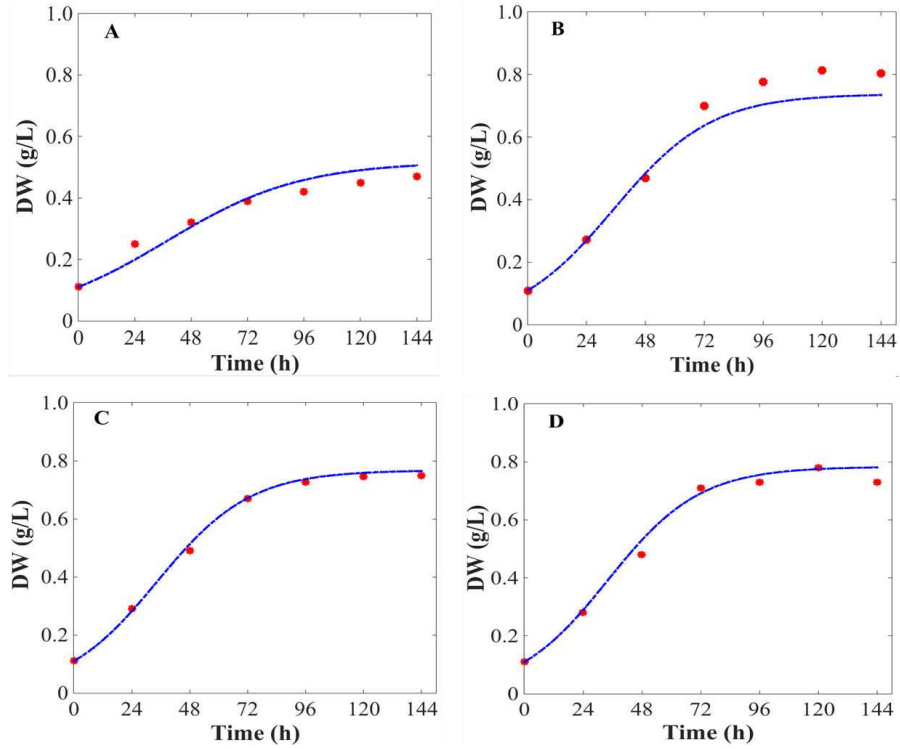
620

621

622

623 **Figure 5.** Comparison of model simulation results and real experimental data of  
624 biomass in *D. salina*. DW, dry weight.

625



626

627

628

629

630

631

632

633

634

635

636

637

638

639

640

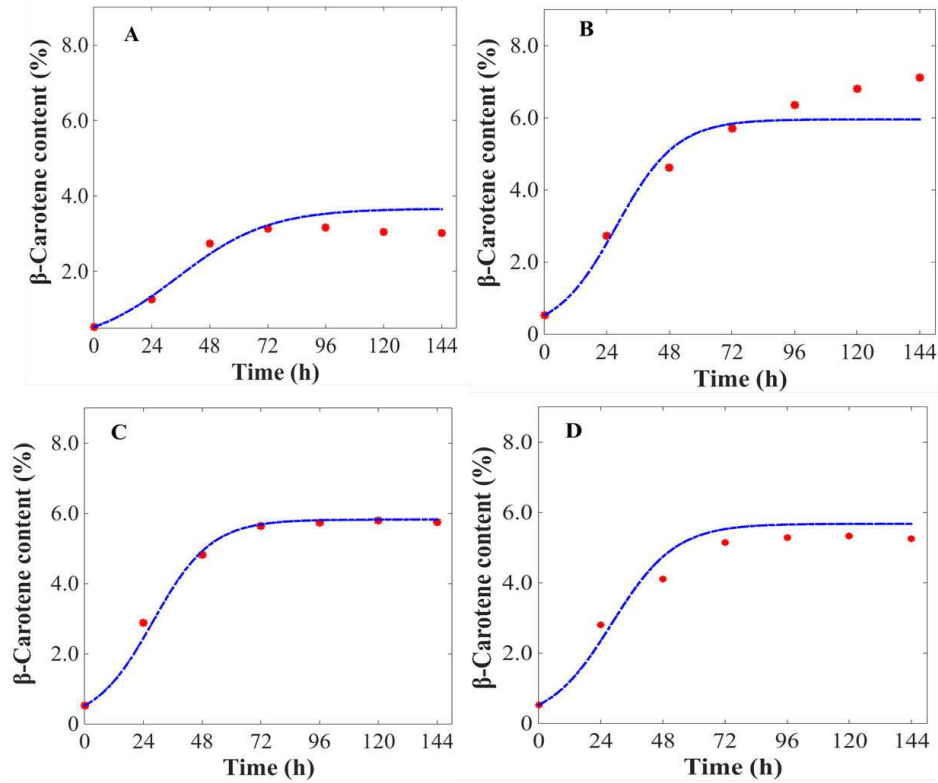
641

642

643

644 **Figure 6.** Comparison of model simulation results and real experimental data of  
645  $\beta$ -carotene content in *D. salina*.

646



647

648

649

650

651

652

653

654

655

656

657

658

659

660

661

662

663

664

665 **Tables**666 **Table 1. Parameters based on average light intensity**

Parameter	Unit	Value
$K_s$	$\mu\text{mol m}^{-2} \text{s}^{-1}$	379.6
$E_a$	$\text{kJ mol}^{-1}$	0.6684
$E_b$	$\text{kJ mol}^{-1}$	0.6449
$E_{aw}$	$\text{kJ mol}^{-1}$	5.286
$E_{bw}$	$\text{kJ mol}^{-1}$	6.069
$K_{sw}$	$\mu\text{mol m}^{-2} \text{s}^{-1}$	580
A	$\text{h}^{-1}$	15.09
B	$\text{h}^{-1}$	14.9
$A_w$	$\text{h}^{-1}$	0.4355
$B_w$	$\text{h}^{-1}$	0.35
$\mu_{\max}$	$\text{h}^{-1}$	0.1608
$\mu_{\max w}$	$\text{h}^{-1}$	0.039
$K_i$	$\mu\text{mol m}^{-2} \text{s}^{-1R}$	1705
$K_{iw}$	$\mu\text{mol m}^{-2} \text{s}^{-1}$	936.5
$k_q$		9.88
$K_C$		0.22
$K_{CW}$		10.38
$k_{qw}$		43.37
b		0.03
$\mu_d$		0.3

667

668

**Table 2. Optimization of model parameters (optimized by MATLAB)**

Parameter	Unit	Value (计算)	优化后
$K_s$	$\mu\text{mol m}^{-2} \text{s}^{-1}$	379.6	384.9
$E_a$	$\text{kJ mol}^{-1}$	0.6684	1.0026
$E_b$	$\text{kJ mol}^{-1}$	0.6449	0.5572
$E_{aw}$	$\text{kJ mol}^{-1}$	5.286	7.9290
$E_{bw}$	$\text{kJ mol}^{-1}$	6.069	3.0345
$K_{sw}$	$\mu\text{mol m}^{-2} \text{s}^{-1}$	580	581.6
A	$\text{h}^{-1}$	15.09	22.6350
B	$\text{h}^{-1}$	14.9	17.4630
$A_w$	$\text{h}^{-1}$	0.4355	0.6533
$B_w$	$\text{h}^{-1}$	0.35	0.1750
$\mu_{\max}$	$\text{h}^{-1}$	0.1608	0.20278
$\mu_{\max w}$	$\text{h}^{-1}$	0.039	0.0405
$K_i$	$\mu\text{mol m}^{-2} \text{s}^{-1}$	1705	1707
$K_{iw}$	$\mu\text{mol m}^{-2} \text{s}^{-1}$	936.5	937.1
$K_N$		9.88	10.23
$K_C$		0.22	0.26
$K_{CW}$		10.38	10.5
$K_{NW}$		43.37	45.98
b		0.03	0.0150
$\mu_d$		0.3	0.15

672 **Table 3.** List of arbitrary cultivation condition parameter value

Photobio reactor	Initial DW (g·L <sup>-1</sup> )	Day/Night (h:h)	Temperature (°C)	Light (μmol m <sup>-2</sup> s <sup>-1</sup> )	Carbon (Mm)	Nitrogen (mg·L <sup>-1</sup> )
a	0.1	14:10	20	200	5	50
b	0.1	24:0	25	600	5	500
c	0.1	24:0	20	800	200	50
d	0.1	14:10	25	1000	200	500

673

## Supplementary Files

This is a list of supplementary files associated with this preprint. Click to download.

- [GraphicalabstractforBIOB.jpg](#)